Unraveling the Origin of Band Shapes in Infrared Spectra of $N_2O-{}^{12}CO_2$ and ${}^{12}CO_2-{}^{13}CO_2$ Ice Particles†

Ruth Signorell,*,‡,§ Martin Jetzki,‡ Marc Kunzmann,‡ and Roman Ueberschaer‡

Institut für Physikalische Chemie, Universität Göttingen, Tammannstrasse 6, D-37077 Göttingen, Germany, and Department of Chemistry, University of British Columbia, 2036 Main Mall, Vancouver, British Columbia V6T 1Z1, Canada

Received: June 7, 2005; In Final Form: July 20, 2005

Band structures in the region of strong infrared absorption bands for different $N_2O-{}^{12}CO_2$ and ${}^{12}CO_2-{}^{13}CO_2$ composite particles are investigated by combining quantum mechanical exciton calculations with systematic experimental investigations. The ice particles are generated by collisional cooling and characterized with rapid−scan infrared spectroscopy. The size of the particles lies between ∼10 and 100 nm. The calculated spectra show excellent agreement with the experimental data. This work leads to a detailed understanding on a molecular level of shape effects in pure and statistically mixed particles as well as of the characteristic features observed for core−shell particles.

1. Introduction

Cold weakly bound molecular aggregates with sizes ranging from less than nanometers up to microns play an important role in various atmospheric processes and in astrophysics as components of interstellar dust.[1,2] In both fields the knowledge of the spectroscopic properties of these ice particles is of central interest. For molecular compounds infrared spectroscopy is particularly well suited since it provides a broad range of information about particle properties. It is of great interest to understand the influence of intrinsic particle properties, such as size, shape, and surface area, on band shapes in infrared spectra, which can exhibit very characteristic features.[3−18] Although nowadays an increasing amount of experimental data is available for ice particles of different composition, the interpretation of the observed spectral signatures is often rather speculative. A detailed understanding is only possible by combining systematic experimental investigations with detailed modeling based on molecular properties.[6,10,15,17,19−22] This is demonstrated in the present contribution for the example of N_2O-CO_2 and ${}^{12}CO_2-{}^{13}CO_2$ composite particles.

To generate large molecular aggregates, expansion techniques[9,11,14,23−37] or cooling cells[3,6,7,10,15,38−47] with various designs are typically used, often in combination with in situ infrared spectroscopy. Pure and composite carbon dioxide ice particles are among the experimentally best investigated particulate systems using these techniques and infrared spectroscopy.[3,5−7,13,14,16,18,27,40,42,46,48−50] Here, special attention has been given to the characteristic band shapes of the antisymmetric stretching−vibration of CO_2 and its dependence on experimental conditions (pressure, temperature, concentration, time evolution, influence of mixing with other substances). Although a large body of experimental data exists for CO_2 aggregates with very different sizes, the interpretation of the various features observed had been the subject of controversial discussions. The main reason for that was the lack of a molecular model that is able to predict infrared spectra of CO_2 aggregates with enough accuracy and that is applicable over the whole size range from small oligomers up to micron sized particles.

For large particles with diameters above about 10 nm (∼10 000 molecules) classical scattering theory[51] can in principle be used to simulate infrared spectra. This method, however, requires as input refractive index data, which have to be obtained from independent experimental investigations. The corresponding data are often not accurate enough to interpret details found in infrared spectra unambiguously. For many multicomponent systems such data are not available at all. Moreover, classical scattering theory gives no insight into the microscopic origin of the observed phenomena, i.e., into the dominant inter- and intramolecular interactions. It had been realized early by different research groups[3,6,19,20,27] that similar to the situation in the solid CO_2 bulk[52] resonant dipole coupling (vibrational exciton coupling) between the different molecules in CO_2 aggregates could be one of the main interactions that determines the band structures of the antisymmetric stretching−vibration. On the basis of this assumption exciton calculations had been performed but only for small particles which contained less than 2000 molecules. The comparison with experimental spectra was not really satisfactory.

To clarify this point we have recently compared vibrational exciton calculations with quantum chemical calculations and extended the exciton approach to treat large particles consisting of many thousands of molecules.[15,21] The comparison of exciton simulations with standard quantum chemical calculations for large CO_2 clusters clearly shows that resonant dipole coupling is indeed by far the most important contribution to the band shapes of strong infrared absorptions.[21] Furthermore, we have demonstrated that calculations for small particles (diameter < 5 nm) are completely inadequate to interpret spectral features observed for large particles (diameter > 10 nm).[15] These results clearly hint that the above-mentioned discrepancies between calculations and experimental data arose not from deficiencies

† Part of the special issue "Jürgen Troe Festschrift".

* Corresponding author fax: (604)822-2847; e-mail: signorell@chem.ubc.ca. Current address: Department of Chemistry, University of British Columbia, 2036 Main Mall, Vancouver, British Columbia V6T 1Z1, Canada.

‡ Universität Göttingen.

§ University of British Columbia.

10.1021/jp053021u CCC: $33.50
Published on Web 09/27/2005

in the model but from the fact that experimental data for large particles were compared with calculations for small particles. It is thus not surprising that our recent investigations in this field, which invariably combine systematic experimental studies with exciton calculations in the appropriate size range, have produced a more consistent picture for many features observed in infrared spectra of pure and composite CO_2 particles. For example, we could show that the temporal evolution and pressure dependence observed in collisional cooling cells for CO_2 particles with sizes above 10 nm is consistent with a change in the particles' shape.[13,15,16] Somewhat simplified we can summarize now that with increasing time after the particle formation and with decreasing bath gas pressure the particles change from globular to more elongated shapes. For the example of statistically mixed $^{12}CO_2-^{13}CO_2$[13] and CO_2-NH_3[16] particles we could solve the puzzle why such shape effects are less prominent for mixed particles. And very recently the exciton model has helped us to elucidate some of the characteristic features observed in the infrared spectra of small CO_2 particles.[49]

The present contribution is devoted to the detailed theoretical and experimental investigation of band shapes observed in the infrared spectra of different $N_2O-^{12}CO_2$ and $^{12}CO_2-^{13}CO_2$ composite particles with sizes above 10 nm. This comprises the study of shape effects in pure and statistically mixed particles and the explanation of infrared signatures observed for core−shell particles.[50,53,54] In both examples, $^{12}CO_2$ is mixed with a second component that also exhibits strong dipole coupling. We will show that the dipole coupling between the two different components can still have a distinct influence on the infrared spectra although the interaction is no more resonant in this case.

2. Experiment and Modeling

The ice particles have been generated in our collisional cooling cells and spectroscopically investigated in situ in the aerosol phase with rapid scan Fourier transform infrared spectroscopy. The main experimental setup has already been described in detail previously.[15,45,46,53,54] A detailed description of our twin chamber cell will be deferred to a forthcoming contribution. Briefly, in cooling cells the particles are formed by injecting a warm dilute sample gas into a cold bath gas which leads to supersaturation and thus to particle formation. For the present contributions, we have used as bath gas helium (Messer 99.999%) at liquid nitrogen temperature (T_{bath}=78 K) and pressures between 200 and 1000 mbar. The sample gas (typically 200−1000 ppm in helium; total pressure 600−2000 mbar) has been introduced into the cells with the help of magnetic valves as single pulses. For the statistically mixed particles, we have used premixed samples and a single pulse of about 2000 ms duration. For the core−shell particles we have used our two-gas-pulse inlet which has been described in detail in ref 53. An analogous design has recently been described in ref 50. The two different sample gases are introduced into the cell through two spatially separated inlet tubes which are connected to two different magnetic valves. Core−shell particles are generated when the opening times of the two valves are shifted in time (typically 500 ms). The size of the particles investigated here lies between ∼10 and 100 nm (see refs 16 and 49). $^{12}CO_2$ (99.5%) and N_2O (99.5%) have been purchased from AGA Gas GmbH and Gerling Holz and Co., respectively. The $^{13}CO_2$ gas was prepared in our laboratory from sodium carbonate (Aldrich, 99% ^{13}C) and sulfuric acid.

Here we use the quantum mechanical exciton approach to calculate infrared spectra in the region of strong absorption bands. For further details of this model we refer to our previous contributions and references therein.[15,21,55] This approach assumes that the coupling between the oscillating dipoles of the individual molecules in a particle is the dominant contribution to the infrared spectra. This is a good approximation if the corresponding molecular transition dipoles are strong (transition dipoles > 0.1−0.2 D) and the next nearest neighbour molecules in the particles are separated by small distances (r_{ij} < 5−7 Å). Both conditions are fulfilled for the vibrational bands and substances considered here. The corresponding vibrational Hamiltonian has the form

$$\hat{H} = \hat{H}_0 + \hat{H}_D$$

$$\hat{H}_D = \sum_{i<j} -\frac{1}{4\pi\epsilon_0}\vec{\mu}_i \cdot \frac{3(\vec{\mu}_j\cdot\vec{r}_{ij})\cdot\vec{r}_{ij} - (\vec{r}_{ij}\cdot\vec{r}_{ij})\cdot\vec{\mu}_j}{r_{ij}^{\,5}} \qquad (1)$$

where $\hat{H}_0$ is the sum over the vibrational Hamiltonians of the uncoupled molecules in a particle. $\hat{H}_D$ includes all pairwise dipole−dipole interactions between the molecules in the aggregate. $\vec{r}_{ij}$ is the distance between the centers of mass of the molecules labeled i and j, and $\vec{\mu}$ is the dipole moment operator. Up to first order terms in the vibrational coordinates, the model contains only two parameters: The transition wavenumber of the uncoupled molecule $\tilde{\nu}_M$ and the transition dipole moment of the uncoupled molecule $\delta\mu = \langle 0|\mu|1\rangle$. Both quantities can be extracted from gas-phase measurements. The diagonalization of $\hat{H}$ leads to the vibrational eigenfunctions (exciton states) ψ_n and the vibrational eigenvalues $\tilde{\nu}_n$ of the particles. From these quantities we have calculated infrared spectra and for spherical particles radial probability density distributions of the exciton states $\rho(\tilde{\nu}_n, r)$ (see section 4). The latter have been calculated as

$$\rho(\tilde{\nu}_n, r) = \int_\theta \int_\phi |\psi_n(r, \theta, \phi)|^2 \sin(\theta) d\theta d\phi \qquad (2)$$

where r, θ, and ϕ are the polar coordinates.

3. $N_2O-^{12}CO_2$ Particles

This section deals with different N_2O-CO_2 composite particles.[54] In the first subsection, we discuss the influence of the degree of mixing on shape effects in infrared spectra for statistically mixed particles. The second part is devoted to the explanation of band shapes in infrared spectra of composite particles with a core−shell structure. In the mid-infrared region, the shape of the strong absorption bands of CO_2 (antisymmetric stretching−vibration υ_3 around 2363 cm^{-1} and bending−vibration υ_2 around 669 cm^{-1}) and N_2O particles (N−N stretching−vibration υ_3 around 2247 cm^{-1} and N−O stretching−vibration υ_1 around 1296 cm^{-1}) are dominated by *resonant* transition dipole−transition dipole coupling (exciton coupling) between the molecules. Here, we focus on the υ_3 bands, but the same features are also observed for the υ_2 and the υ_1 band. Dipole coupling also acts between the two different substances in composite particles, but in this case the interaction is no longer resonant. In general it therefore has only a minor or even negligible influence on the infrared spectra compared with the interaction between molecules of the same substance. The CO_2 and N_2O particles considered here are crystalline and have very similar crystal structures.[56] Thus we assume that for the composite particles differences due to the slightly different crystal structures are negligible. The size of the particles lies between ∼10 and 100 nm. This has been estimated from dilution experiments combined with scattering calculations in analogy to the procedures described in refs 15 and 16. Note that in this

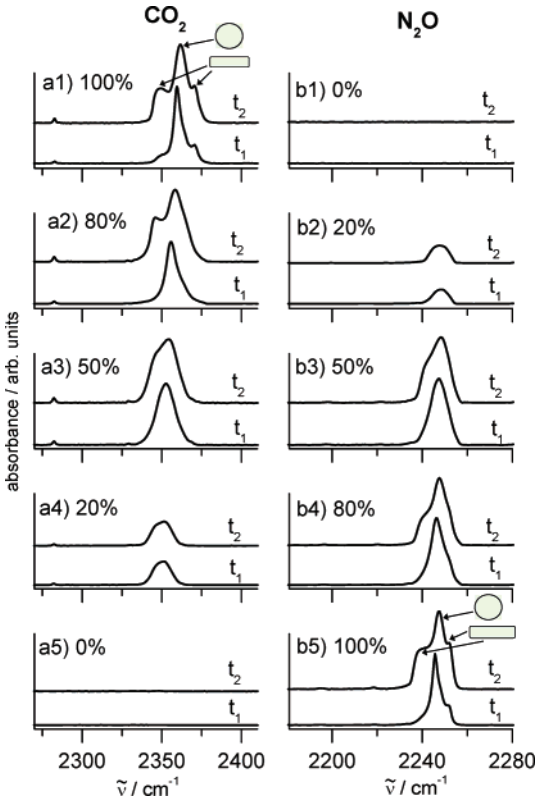

Figure 1. Experimental infrared spectra of statistically mixed N_2O-CO_2 ice particles (T_{bath}=78 K). The composition of the mixture is indicated in each panel. Panels a1−a5: Region of the antisymmetric stretching−vibration υ_3 of CO_2. Panels b1−b5: Region of the N−N stretching−vibration υ_3 of N_2O. t_1: Spectra recorded directly after the particle formation. t_2: Spectra recorded 99 s after the particle formation.

size region the band structure and the relative band intensities are almost completely independent from the particle size[15,51] so that all nontrivial size effects are negligible in this size range. This property makes such systems particularly well suited for the study of shape effects and of the influence of coating.

3.1. Shape Effects. Figure 1 shows shape effects in the infrared spectra of various pure and statistically mixed N_2O-CO_2 ice particles. The region of the υ_3 band of CO_2 is depicted in panels a1−a5. Panels b1−b5 illustrated the evolution of the υ_3 band of N_2O for the same particles. As indicated in the figure, the mole fraction of CO_2 decreases, and the mole fraction of N_2O increases continually from top to bottom. Panel a1 shows the characteristic temporal evolution observed for pure CO_2 particles. The spectrum in the lower trace of panel a1 was measured directly ($t_1 = 0$ s) after the particle formation, and the spectrum in the upper trace was recorded 99 s ($= t_2$) later. Immediately after the particle formation the spectrum consists of a single strong band and two weak shoulders on both sides. With increasing time, the intensities of the two shoulders continually increase compared with the central peak. Exactly the same temporal behavior is also observed for the υ_3 band of pure N_2O particles (panel b5) as well as for the υ_2 and the υ_1 band (not shown here) of CO_2 and N_2O, respectively. In a previous contribution,[13] we have shown with the help of exciton calculations that the temporal evoluation of the infrared bands can be explained consistently by a temporal change of the particles shape: With increasing time the particles evolve from globular shapes, which are characterized by the central peak, to more elongated particles, which cause the two shoulders on both sides. We still do not have a conclusive answer as to the mechanism behind the formation of the different particle shapes.

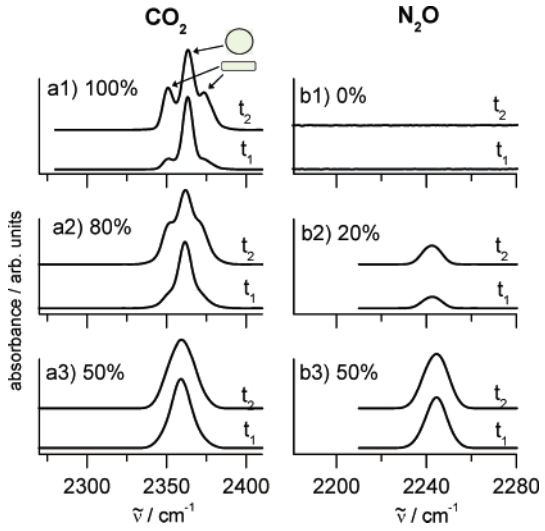

Figure 2. Calculated infrared spectra of statistically mixed N_2O-CO_2 ice particles. All calculations were performed with the exciton approach. Panels a1−a3 and b1−b3 show the simulations corresponding to the same panels of Figure 1. The calculated spectra for the two different times t_1 and t_2 only differ in the ratio of globular and elongated particles. This ratio amounts to 2:1 and 2:6 at t_1 and t_2, respectively. The simulations confirm an evolution from predominantly globular to elongated particle shapes with time.

Elongated particles could be produced by agglomeration of globular primary particles or by evaporation of small primary particles and subsequent dendritic growth of larger primary particles. The fact that we find the same behavior for the N_2O (panel b5) and for the CO_2 (panel a1) band clearly supports our previous conclusion that resonant dipole coupling is the main reason for the shape sensitivity of the band structures. Both vibrational transitions have strong molecular transition dipoles ($\delta\mu$=0.32 and 0.25 D for CO_2 and N_2O, respectively[57,58]), and the next nearest neighbour molecules within the particles are separated by short distances (r_{ij} < 5 Å) (see eq 1 and refs 21 and 55).

The shape sensitivity of the absorption bands should decrease for statistically mixed particles compared with pure particles if resonant transition dipole coupling is the dominant interaction. In analogy to our previous results for statistically mixed $^{12}CO_2-{}^{13}CO_2$ particles[13] we expect that with increasing dilution the absorption bands become single broad unstructured bands which at higher dilution (>50%) are no longer sensitive to the particles' shape. The reason is that in mixed particles the distance (r_{ij}) between the same type of molecules increases so that the effect of resonant transition dipole coupling is reduced (see eq 1). This is exactly what we observe for the statistically mixed N_2O-CO_2 particles in Figure 1 in panels a2−a4 and b4−b2: The more dilute one component is, the less structured is its absorption band. At higher dilutions (>50%) the bands are indeed virtually independent from the shape of the particles, i.e., there is no difference between the two spectra measured at times t_1 and t_2.

The experimental trends described above are fully confirmed by exciton calculations for pure and statistically mixed particles. As an example, Figure 2 shows the corresponding simulations for panels a1−a3 and b1−b3 of Figure 1. For these simulations we have used the following values for the transition wavenumbers $\tilde{\nu}_M$ and the transition dipole moments $\delta\mu$ of the uncoupled molecules (see eq 1 and refs 13, 55, 57, and 58):

$$\tilde{\nu}_M(^{12}CO_2) = 2355\ \text{cm}^{-1} \quad \text{and} \quad \delta\mu(^{12}CO_2) = 0.32\ \text{D}$$

$$\tilde{\nu}_M(N_2O) = 2242\ \text{cm}^{-1} \quad \text{and} \quad \delta\mu(N_2O) = 0.25\ \text{D} \quad (3)$$

All model particles have the cubic crystal structures of the bulk at 78 K[56] and consist of ~14 000 molecules ($d \approx 10$ nm). From about 10 to 100 nm the band shapes in infrared spectra are to a good approximation size-independent (refs 15 and 16; electrostatic approximation[51]). We have tested the convergence of our calculated spectra with respect to size by systematically increasing the number of molecules per particle. The model particles considered here are thus a reliable representation of the experimentally generated particles whose sizes are estimated to lie in this range. As noted above, we have interpreted the temporal evolution observed in the spectra in terms of a change of the particle shape: At short times (t_1) predominantly globular particles are observed, whereas at longer times (t_2) the portion of elongated particles increases more and more. For the simulations the globular particles are represented by a sphere and the elongated particles by two rectangular parallelepipeds with axes ratios of 3:1:1 and 6:1:1, respectively. For all calculations, the ratio of globular to elongated particles has been set to be 2:1 at time t_1 and 2:6 at time t_2. The portion of the two different parallelepipeds is equal. The important metric here is not the exact shape, but the fact that the spectrum of globular particles (central peak in the spectra in panel a1) can be distinguished clearly from the spectrum of elongated particles (two shoulders around the central peak). For the elongated particles we have used two different axes ratios to illustrate that even a change in its value by a factor of 2 does not wipe out the differences between globular and elongated particles in the case of pure particles.[13] The comparison of Figures 1 and 2 finally shows that the dependence of spectra on the particle shape (time evolution) and on the degree of mixing are indeed nicely reproduced by the calculations. This clearly demonstrates exciton coupling to be the dominant interaction. Note that our aim is not to reproduce all details of the experimental spectra but to explain the general trends by as simple a model as possible. Of course, a perfect agreement could easily be achieved for instance by mixing many particle shapes. This, however, would only improve the aesthetics of the presentation and not our understanding of the general trend.

3.2. Core-Shell Particles. If exciton coupling is the dominant interaction it should also explain the infrared spectra of other composite particles, for instance of particles with a core−shell architecture. That this is indeed the case is illustrated for different N_2O-CO_2 core−shell particles by Figure 3. We concentrate here on spherical particles. The advantage of spherical particles is that *pure* spherical particles only show a single absorption band in contrast to other particles shapes which lead to more complex band shapes (see previous subsection). For the examples of spheres, the effect of coating can thus be elucidated very clearly.

Calculated infrared spectra for different core−shell particles are depicted in panels a1−c1 in Figure 3. All three examples show that the spectrum of the core consists of a single band as is the case for pure spheres. The shells essentially lead to two different absorption bands similar to what is found for thin layers.[20] The intensity ratios and the exact band shapes of the shell spectra, however, depend on the relative absorption frequencies of the two substances (panels a1 and b1) and the portion of the shell (panels b1 and c1). The dependence on the relative absorption frequencies may be somewhat surprising. It can be traced back to a *nonresonant* coupling effect between shell and core. Both phenomena are discussed and explained further in the following section for the example of $^{12}CO_2-^{13}CO_2$ particles for which exactly the same effects occur. The calculations in panels a1−c1 demonstrate that detailed information on such core−shell particles can be extracted from infrared spectra.

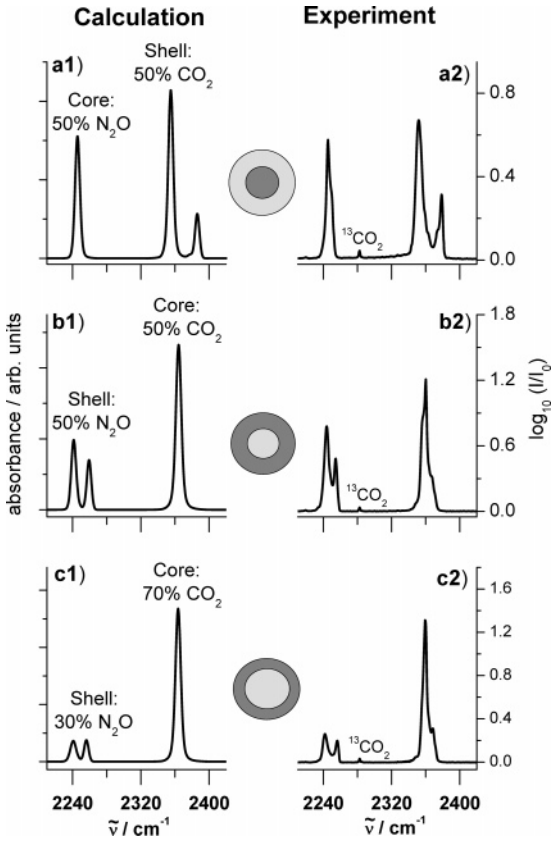

Figure 3. Panels a1−c1: Vibrational exciton calculations for different N_2O-CO_2 core−shell particles with spherical shapes. The structure and composition of the particles is indicated in the figure. Panels a2−c2: Corresponding experimental infrared spectra (T_{bath}=78 K). The $^{13}CO_2$ peaks arise from the natural abundance of $^{13}CO_2$ (~1%) in $^{12}CO_2$.

The corresponding experimental spectra are depicted in panels a2−c2. The experimental conditions have been chosen so as to form predominantly globular particles as described in the previous section and in refs 13 and 16. To generate the core−shell particles we have used our two−gas−pulse inlet described in more detail in section 2 and ref 53. For the present measurements, the time delay between the first pulse, which generates the cores, and the second pulse, which coats them, amounted to about 500 ms. Figure 3 shows a good agreement between calculated and experimental spectra. All essential features described above for the calculations are indeed observed in the experimental spectra. The small deviations of the experimental data from the ideal behavior of spherical core−shell particles can be traced back to two main reasons: (1) The fact that not all particles generated have an ideal spherical shape explains why the bands, in particular of the cores, still show some fine structure in the experimental spectra. (2) The separation of the two bands of the shells is less clear in the experimental spectra. This hints to the fact that the second pulse not only coats the core particles but also leads to a very small amount of pure particles. These pure particles absorb exactly between the two bands of the shell. Points (1) and (2) also explain the slight deviations observed for the relative absorbances of different bands between experiment and simulation. The results in Figure 3 nicely demonstrate that it is possible to generate ice nanoparticles of a certain architecture in the lab, and in particular it elucidates that their spectra can be perfectly predicted and understood in terms of molecular interactions.

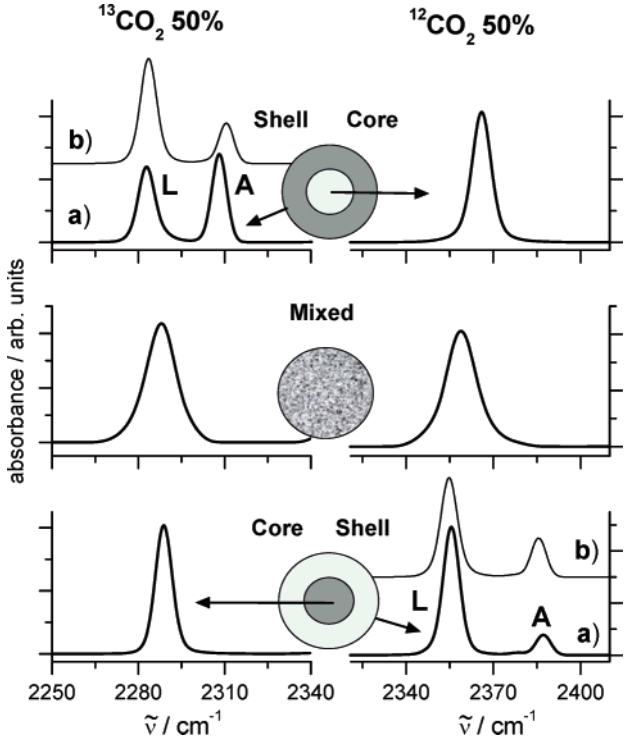

Figure 4. Calculated infrared spectra of $^{12}CO_2-^{13}CO_2$ composite particles in the region of the antisymmetric stretching−vibrations of $^{13}CO_2$ (left-hand side) and $^{12}CO_2$ (right-hand side). The ratio of the two isotopomers amounts to 1:1 for all spectra. Upper panel: $^{13}CO_2$ shell with $^{12}CO_2$ core. Middle panel: Statistically mixed particles. Lower panel: $^{12}CO_2$ shell with $^{13}CO_2$ core. Traces b in the upper and lower panels show the spectra of shells which do not couple to the core.

4. $^{12}CO_2-^{13}CO_2$ Particles

The same behavior as described in the previous section for N_2O-CO_2 particles has also been found for $^{12}CO_2-^{13}CO_2$ composite particles. In a previous publication,[13] we have investigated shape effects in infrared spectra of pure and statistically mixed $^{12}CO_2-^{13}CO_2$ particles and verified the observed features by exciton calculations. Since transition dipole coupling is the dominant interaction in these systems as well, it is not surprising that the same features have been found in the infrared spectra as described in section 3.1 for statistically mixed N_2O-CO_2 ice particles. $^{12}CO_2-^{13}CO_2$ core−shell particles have been measured previously,[53,50] but up to now their interpretation in terms of a microscopic model had been missing. The main goal of the present section is to fill this gap.

Recently, Bauerecker[50] has published detailed spectra in the region of the antisymmetric stretching−vibrations for $^{12}CO_2-^{13}CO_2$ core−shell particles and statistically mixed particles with a 1:1 ratio of the two isotopomers. To explain the main features observed in these spectra we start here with calculations for such 1:1 particles (see Figure 4). The main spectral signatures observed experimentally for these particles have been summarized in Figure 3 of ref 50. They are essentially the same as observed for the N_2O-CO_2 particles in the previous section (see Figure 1 panels a3 and b3 and Figure 3 panels a and b). For statistically mixed particles both isotopomers exhibit more or less a single band as we have previously shown both experimentally and by exciton calculations in ref 13. In the spectra of the 1:1 $^{12}CO_2/^{13}CO_2$ core−shell and the 1:1 $^{13}CO_2/^{12}CO_2$ core−shell particles in ref 50 shape effects were not completely eliminated, but the general features of core−shell particle spectra are still evidently the same as described in section 3.2 (see Figure 3) for N_2O-CO_2 particles: The spectra of the cores consist of a single band, whereas the shells lead to two different absorption bands. The high-frequency band of the shell is labeled A in the spectra in ref 50. The low−frequency band of the shell was not labeled there probably because it is difficult to distinguish from the R-bands in these spectra. For clarity, we label them L in the following. Note that other features in the spectra in ref 50, as for instance the R and B peaks, arise from shape effects in accordance with the temporal evolution as explained above in section 3.1. An interesting point is that in the experimental spectra, the A:L peak intensity ratio for the $^{12}CO_2/^{13}CO_2$ core−shell particles is higher than for the $^{13}CO_2/^{12}CO_2$ core−shell particles. We have observed the same behavior in section 3.2 for N_2O-CO_2 core−shell particles. Figure 4 shows the exciton calculations for spherical $^{12}CO_2-^{13}CO_2$ composite particles with a 1:1 ratio of the two isotopomers. The parameters used for $^{12}CO_2$ are given in eq 3. The corresponding values for $^{13}CO_2$ are taken from ref 13 to be

$$\tilde{\nu}_M(^{13}CO_2) = 2284\ \text{cm}^{-1} \quad \text{and} \quad \delta\mu(^{13}CO_2) = 0.30\ \text{D} \quad (4)$$

Here we consider only spherical particles because all important features observed for core−shell particles are already contained in these spectra. The middle panel in Figure 4 depicts the spectrum of statistically mixed particles for which both isotopomers exhibit a single band in accordance with the experimental spectra. The two different core−shell particles (traces a in the top and bottom panel of Figure 4) lead to a single peak for the core and to two characteristic absorption bands for the shell as noted above for the experimental spectra. In nice agreement with the experimental spectra, the relative intensity of the A-peak is higher for the $^{12}CO_2/^{13}CO_2$ particles (trace a in the top panel of Figure 4) than for the $^{13}CO_2/^{12}CO_2$ particles (trace a in the bottom panel). As already mentioned in section 3.2 this behavior can be explained by a *nonresonant* coupling between shell and core. For shells which do not couple to the core one gets the spectra which are depicted in traces b of the top and the bottom panel in Figure 4. The intensity distributions between the two shell bands clearly differ from those of shells which couple to the cores (traces a). This illustrates that although nonresonant the coupling of the shell to the core is not negligible in this specific case.

The lower panels of Figures 5−7 give an impression of how the radial probability density distributions of exciton states for different spherical particles behave (see eq 2). The upper panels again show the corresponding infrared spectra. Figure 5 elucidates that a pure CO_2 sphere has a single absorption band (upper panel) and in particular that the exciton states are delocalized over the whole particle (lower panel). This delocalization explains the distinct shape and size dependence of exciton states. The results for a pure sphere are consistent with the corresponding results from classical scattering theory.[51] In a classical picture, the normal mode which leads to the single absorption band in Figure 5 is called the Fröhlich mode. There is no radial variation of the radial component of the electric field for this mode. It is thus called the mode of uniform polarization. Our exciton calculations obviously reproduce the classical limit. But in contrast to the classical approach, the exciton approach does not rely on input data such as refractive index data, and in particular it provides a microscopic explanation of the observed phenomena. Furthermore, the quantum mechanical approach can also be used for even smaller particles[15,49] where classical scattering theory is no more valid. Figure 6 illustrates what happens with the probability density in $^{12}CO_2/^{13}CO_2$ core−shell particles. The delocalization is now confined to two different regions: the shell and the core. The

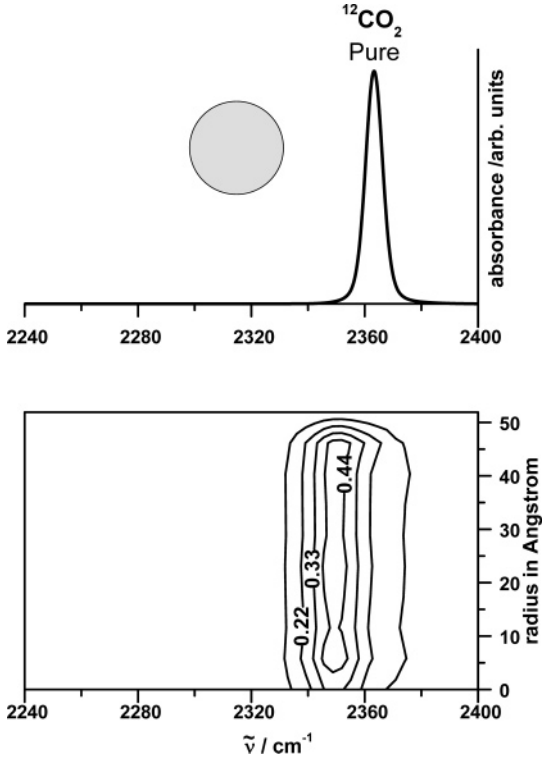

Figure 5. Upper panel: Calculated infrared spectrum of a pure $^{12}CO_2$ sphere in the region of the antisymmetric stretching−vibration. Lower panel: Radial probability density distribution of the exciton states (see eq 2).

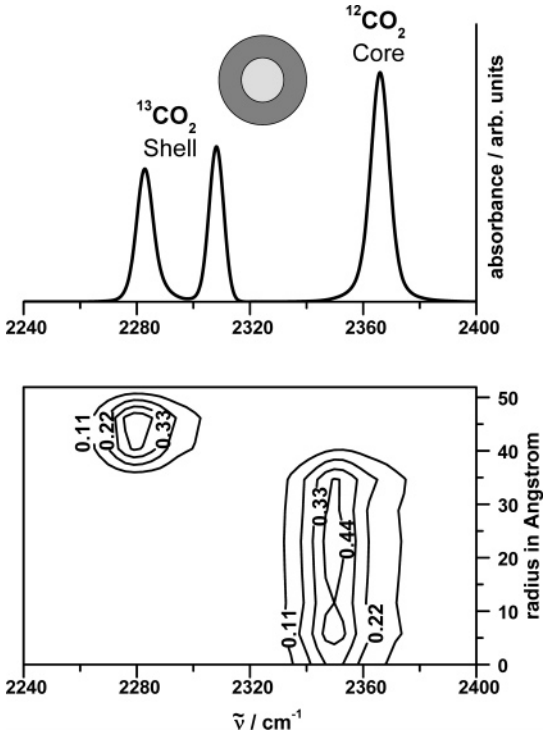

Figure 6. Upper panel: Calculated infrared spectrum of a $^{12}CO_2/^{13}CO_2$ core−shell particle in the region of the antisymmetric stretching−vibrations (see also upper panel in Figure 4). The ratio of the two isotopomers amounts to 1:1. Lower panel: Radial probability density distribution of the exciton states (see eq 2).

reason for this confinement comes from the fact that the resonant coupling only acts within these two regions. Consistent with this, for statistically mixed $^{12}CO_2-^{13}CO_2$ particles one finds again a delocalization over the whole particle for both absorptions of the two isotopomers. This is illustrated in Figure 7. Compared with a pure particle (Figure 5) the total probability density is, however, distributed between the two bands.

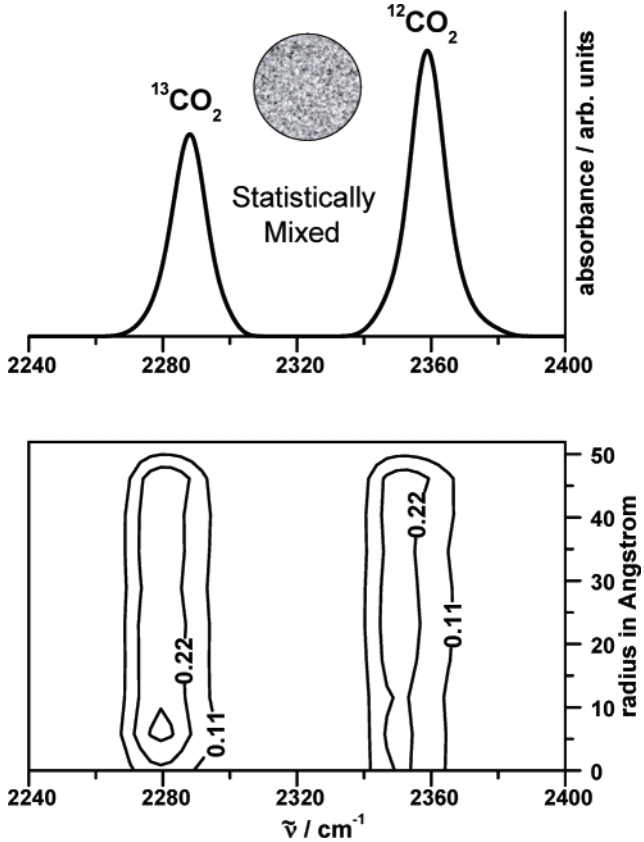

Figure 7. Upper panel: Calculated infrared spectrum of a statistically mixed $^{12}CO_2-^{13}CO_2$ particle in the region of the antisymmetric stretching−vibrations (see also middle panel in Figure 4). The ratio of the two isotopomers amounts to 1:1. Lower panel: Radial probability density distribution of the exciton states (see eq 2).

The spectral signatures of core−shell particles also depend strongly on the ratio of core and shell. This is illustrated by exciton calculations in Figure 8 for spherical particles with $^{12}CO_2$ cores and $^{13}CO_2$ shells. The spectrum of the shell (left-hand side) changes characteristically with the shell thickness. If the shell is much thinner than a unit cell, i.e., if in fact the shell molecules cover the core only sparsely, the shell spectrum consists of a single absorption band near the frequency of the isolated molecules (trace a in Figure 8). For shell thicknesses in the region of one to several unit cells (traces b−d), the spectra resemble those of thin layers with essentially two bands.[20] The spectrum of a pure particle is again found as soon as the shell becomes very thick compared with the core (trace e). The spectra of the core (right-hand side of the figure) are nearly independent of the thickness of the shell. If the core itself is not too small ($r > 2-3$ nm; traces a−d), then its spectrum consists of a single band as found for pure spheres without coating. Compared with pure particles, only the position shifts slightly for thicker shells. For very small cores ($r < 2-3$ nm) the spectrum becomes more complex as described in ref 15. This is a size effect which in the case of core−shell particles is somewhat modified compared with pure particles by the presence of the shell.

Typical experimental spectra for core−shell particles with portions of the shell of more than 10% have already been shown in section 3.2. For completeness, we thus only show here two experimental spectra for core−shell particles with only sparsely covered cores (<2%) in Figure 9.[53] Only the absorption bands for the shells are depicted in the figure. Trace a in Figure 9

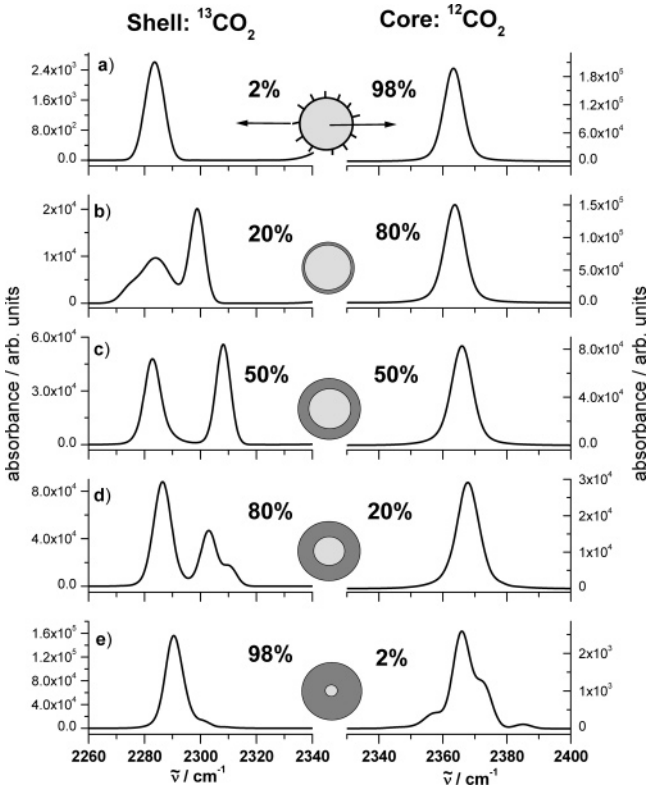

Figure 8. Calculated spectra for $^{12}CO_2/^{13}CO_2$ core−shell particles with different composition. From trace a to trace e the portion of the shell increases systematically. The overall size of the sphere is held fixed for all five cases.

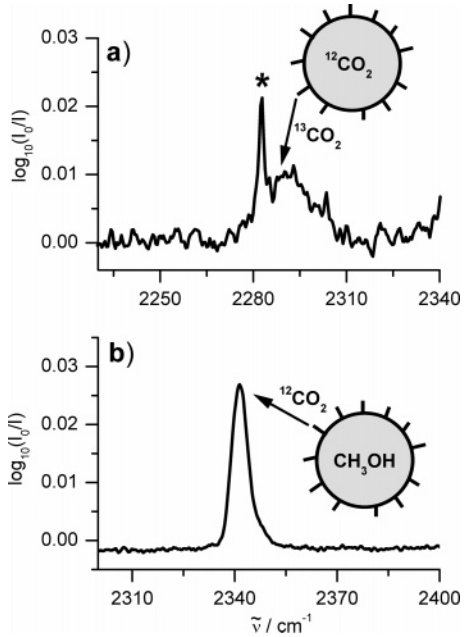

Figure 9. Trace a: Experimental infrared spectrum of $^{12}CO_2/^{13}CO_2$ core−shell particles in the region where the shell ($^{13}CO_2$) absorbs (T_{bath}=78 K). Trace b: Experimental infrared spectrum of methanol/$^{12}CO_2$ core−shell particles in the region where the shell ($^{12}CO_2$) absorbs (T_{bath}=78 K). In both cases, the cores are only sparsely covered with shell molecules. The percentage of shell molecules amounted to less than 2%.

contains the spectrum of the shell of $^{12}CO_2/^{13}CO_2$ core−shell particles, and trace b shows the spectral structure of methanol/$^{12}CO_2$ core−shell particles. According to trace a in Figure 8 one expects one single absorption band for the shell part for such sparsely covered particles. For the methanol/$^{12}CO_2$ particles in trace b of Figure 9 this is fulfilled. The exact position and band shape depend on the intermolecular interactions between $^{12}CO_2$ and methanol and shall not be further discussed here. The $^{12}CO_2/^{13}CO_2$ particles in trace a, however, obviously show two bands and not a single absorption in the region where $^{13}CO_2$ absorbs: a sharp absorption at lower frequencies, which is labeled with an asterisk, and a very broad band at higher frequencies. The low-frequency band does not arise from the $^{13}CO_2$ molecules in the shell. This sharp absorption comes from the natural abundance of $^{13}CO_2$ (∼1%) in the $^{12}CO_2$ core. It is thus not astonishing that this band is also found for pure $^{12}CO_2$ particles. Our simulations show that the $^{13}CO_2$ molecules in the shell absorb blue shifted compared with the $^{13}CO_2$ molecules in the $^{12}CO_2$ cores so that it seems plausible that the broad absorption is due to shell molecules. The comparison with the calculations, however, reveals that the experimentally observed band is much too broad to be explained only by absorptions from shell molecules. As we have already mentioned in section 3.2, the second pulse leads also to the formation of pure particles and does not only cover the core particles. Therefore, we believe that the broad band in trace a is a superposition of $^{13}CO_2$ molecules in the shell and pure $^{13}CO_2$ particles. This is also confirmed by our calculations which predicts that the pure $^{13}CO_2$ particles absorb blue shifted by several cm^{-1} compared with the $^{13}CO_2$ molecules in the shell.

5. Summary

The present investigation demonstrates that infrared spectra of weakly bound molecular ice particles with sizes between 10 and 100 nm contain detailed information about the shape, the mixing effects, and the architecture of the particles. We have shown that collisional cooling techniques allow us to generate different kinds of particles with various particle shapes and architectures such as core−shell particles. The preparation of the particles and the in situ characterization with infrared spectroscopy, however, is only a first step toward a reliable understanding of the various features observed in the spectra. To go beyond the often only speculative interpretations of particle spectra it is indispensable to compare the experimental data with appropriate model calculations. As demonstrated in this contribution, such calculations have to be based on molecular properties (quantum mechanical models) and have to be performed for the correct particle size range. Continuum models are often not accurate enough, and simulations for the wrong size range lead to wrong interpretations.

Together with our previous investigations,[13,15,16,49,53,54] the present results lead to a comprehensive understanding of shape effects and the influence of mixing on them for various pure and statistically mixed ice particles containing N_2O, CO_2, NH_3, SO_2, SF_6, and different isotopomers. The band structure of the strong mid-infrared bands of these particles invariably exhibits the same dependence on the particles' shape and on the mixing ratio. As outlined in this study, such a common behavior is also found for the spectral features of core−shell particles of these substances. Our exciton model reveals that these general trends arise from the transition dipole-transition dipole coupling which acts between all molecules in a particle. In summary, these examples show that intrinsic particle properties can lead to general spectroscopic features and that these spectral signatures can be understood on a molecular level even for particles containing many thousands of molecules.

Acknowledgment. Financial support was provided by the Deutsche Forschungsgemeinschaft (grant Nrs. SI 833/1-1/2, SFB 602, and GRK 782) and by the Fonds der Chemischen Industrie.

References and Notes

(1) Seinfeld, J. H.; Pandis, S. N. *Atmospheric Chemistry and Physics*; Wiley & Sons: New York, 1998.
(2) Ehrenfreund, P.; Charnley, S. B. *Annu. Rev. Astron. Astrophys.* **2000**, *38*, 427−483.
(3) Fleyfel, F.; Devlin, J. P. *J. Phys. Chem.* **1989**, *93*, 7292−7294.
(4) Rowland, B.; Devlin, J. P. *J. Chem. Phys.* **1991**, *94*, 812−813.
(5) Gough, T. E.; Wang, T.-Y. *Chem. Phys. Lett.* **1993**, *207*, 517−520.
(6) Disselkamp, R.; Ewing, G. E. *J. Chem. Phys.* **1993**, *99*, 2439−2448.
(7) Gough, T. E.; Wang, T. *J. Chem. Phys.* **1996**, *105*, 4899−4904.
(8) Clapp, M. L.; Miller, R. E. *Icarus* **1993**, *105*, 529−536.
(9) Häber, Th.; Schmitt, U.; Suhm, M. A. *Phys. Chem. Chem. Phys.* **1999**, *1*, 5573−5582.
(10) Devlin, J. P.; Joyce, C.; Buch, V. *J. Phys. Chem. A* **2000**, *104*, 1974−1977.
(11) Häber, Th.; Schmitt, U.; Emmeluth, C.; Suhm, M. A. *Faraday Discuss.* **2001**, *118*, 331−359.
(12) Kunzmann, M. K.; Bauerecker, S.; Suhm, M. A.; Signorell, R. *Spectrochim. Acta A* **2003**, *59*, 2855−2865.
(13) Signorell, R.; Kunzmann, M. K. *Chem. Phys. Lett.* **2003**, *371*, 260−266.
(14) Bonnamy, A.; Georges, R.; Benidar, A.; Boissoles, J.; Canosa, A.; Rowe, B. R. *J. Chem. Phys.* **2003**, *118*, 3612−3621.
(15) Signorell, R. *Mol. Phys.* **2003**, *101*, 3385−3399.
(16) Jetzki, M.; Bonnamy, A.; Signorell, R. *J. Chem. Phys.* **2004**, *120*, 11775−11784.
(17) Steinbach, C.; Andersson, P.; Kazimirski, J. K.; Buck, U.; Buch, V.; Beu, T. A. *J. Phys. Chem. A* **2004**, *108*, 6165−6174.
(18) Taraschewski, M.; Cammenga, H. K.; Tuckermann, R.; Bauerecker, S. *J. Phys. Chem. A* **2005**, *109*, 3337−3343.
(19) Cardini, G.; Schettino, V.; Klein, M. L. *J. Chem. Phys.* **1989**, *90*, 4441−4449.
(20) Disselkamp, R.; Ewing, G. E. *J. Chem. Soc., Faraday Trans.* **1990**, *86*, 2369−2373.
(21) Signorell, R. *J. Chem. Phys.* **2003**, *118*, 2707−2715.
(22) Häber, Th.; Kevorkiants, R.; Thiel, W.; Suhm, M. A. *Phys. Chem. Chem. Phys.* **2004**, *6*, 4939−4949.
(23) Abraham, O.; Kim, S.-S.; Stein, G. D. *J. Chem. Phys.* **1981**, *75*, 402−411.
(24) Miller, R. E.; Watts, R. O.; Ding, A. *Chem. Phys.* **1984**, *83*, 155−169.
(25) Bartell, L. S. *Chem. Rev.* **1986**, *86*, 492−505.
(26) Bartell, L. S.; Harsanyi, L.; Valente, E. J. *J. Phys. Chem.* **1989**, *93*, 6201−6205.
(27) Barnes, J. A.; Gough, T. E. *J. Chem. Phys.* **1987**, *86*, 6012−6017.
(28) Gauthier, M. *J. Chem. Phys.* **1988**, *88*, 5439−5449.
(29) Barth, H.-D.; Huisken, F. *Chem. Phys. Lett.* **1990**, *169*, 198−203.
(30) Huang, J.; Bartell, L. S. *J. Phys. Chem.* **1994**, *98*, 4543−4550.
(31) Huang, J.; Bartell, L. S. *J. Phys. Chem.* **1995**, *99*, 3924−3931.
(32) Torchet, G.; deFeraudy, M.-F.; Boutin, A.; Fuchs, A. H. *J. Chem. Phys.* **1996**, *105*, 3671−3678.
(33) Tanimura, S.; Okada, Y.; Takeuchi, K. *J. Phys. Chem.* **1996**, *100*, 2842−2848.
(34) Buck, U.; Krohne, R.; Schütte, S. *J. Chem. Phys.* **1997**, *106*, 109−115.
(35) Brudermann, J.; Lohbrandt, P.; Buck, U.; Buch, V. *Phys. Rev. Lett.* **1998**, *13*, 2821−2824.
(36) Streletzky, K. A.; Zvinevich, Y.; Wyslouzil, B. E.; Strey, R. *J. Chem. Phys.* **2002**, *116*, 4058−4070.
(37) Bonnamy, A.; Hermsdorf, D.; Ueberschaer, R.; Signorell, R. *Rev. Sci. Instrum.* **2005**, *76*, 053904.
(38) Dunder, T.; Miller, R. E. *J. Chem. Phys.* **1990**, *93*, 3693−3703.
(39) Barnes, J. A.; Gough, T. E.; Stoer, M. *Rev. Sci. Instrum.* **1989**, *60*, 406−409.
(40) Barnes, J. A.; Gough, T. E.; Stoer, M. *J. Chem. Phys.* **1991**, *95*, 4840−4844.
(41) Clapp, M. L.; Miller, R. E.; Worsnop, D. R. *J. Phys. Chem.* **1995**, *99*, 6317−6326.
(42) Newnham, D.; Ballard, J.; Page, M. *Rev. Sci. Instrum.* **1995**, *66*, 4475−4481.
(43) Bertram, A. K.; Sloan, J. J. *J. Geophys. Res.* **1998**, *103*, 3553−3561.
(44) Niedziela, R. F.; Norman, M. L.; DeForest, C. L.; Miller, R. E.; Worsnop, D. R. *J. Phys. Chem. A* **1999**, *103*, 8030−8040.
(45) Bauerecker, S.; Taraschewski, M.; Weitkamp, C.; Cammenga, H. K. *Rev. Sci. Instrum.* **2001**, *72*, 3946−3955.
(46) Kunzmann, M. K.; Signorell, R.; Taraschewski, M.; Bauerecker, S. *Phys. Chem. Chem. Phys.* **2001**, *3*, 3742−3749.
(47) Dohm, M. T.; Potscavage, A. M.; Niedziela, R. F. *J. Phys. Chem. A* **2004**, *108*, 5365−5376.
(48) Hernandez, J.; Uras, N.; Devlin, J. P. *J. Phys. Chem. B* **1998**, *102*, 4526−4535.
(49) Bonnamy, A.; Georges, R.; Hugo, E.; Signorell, R. *Phys. Chem. Chem. Phys.* **2005**, *7*, 963−969.
(50) Bauerecker, S. *Phys. Rev. Lett.* **2005**, *94*, 033404.
(51) Bohren, C. F.; Huffman, D. R. *Absorption and Scattering of Light by Small Particles*; Wiley-Interscience: New York, 1998.
(52) Decius, J. C.; Hexter, R. M. *Molecular Vibrations in Crystals*; McGraw-Hill: 1977.
(53) Kunzmann, M. K. Doctoral Thesis, Cuvillier Verlag, Göttingen, 2002.
(54) Jetzki, M. Doctoral Thesis, Cuvillier Verlag, Göttingen, 2005.
(55) Bonnamy, A.; Jetzki, M.; Signorell, R. *Chem. Phys. Lett.* **2003**, *382*, 547−552.
(56) Wyckoff, R. W. G. *Crystal Structures*; John Wiley and Sons: New York, 1963; Vol. 1.
(57) Rothman, L. S.; Benedict, W. S. *Appl. Opt.* **1978**, *17*, 2605−2611.
(58) Kagann, R. H. *J. Mol. Spectrosc.* **1982**, *95*, 297−305.